Journal of Materials Research and Technology 28 (2024) 3507–3513

Contents lists available at ScienceDirect

Journal of Materials Research and Technology

journal homepage: www.elsevier.com/locate/jmrt

Effect of cube texture on local softening of friction stir welded joints for nanostructured AA2024 processed by accumulative roll bonding

Majid Naseri [a,*], Mohammad Alvand [b], Ehsan Ahmadi [c], Seyedmehdi Hosseini [d,**], Davood Gholami [c], Abdel-Hamid I. Mourad [e,f,***], Ehsan Borhani [g,****]

[a] South Ural State University, 76 Lenin Av., Chelyabinsk 454080, Russia
[b] Faculty of Materials and Metallurgical Engineering, Semnan University, Semnan, Iran
[c] School of Metallurgy and Materials Engineering, Iran University of Science and Technology (IUST), Narmak, Tehran, Iran
[d] Brunel Centre for Advanced Solidification Technology (BCAST), Brunel University London, Uxbridge, UB8 3PH, UK
[e] Mechanical and Aerospace Engineering Department, College of Engineering, United Arab Emirates University, Al-Ain 15551, United Arab Emirates
[f] National Water and Energy Center, United Arab Emirates University, Al-Ain 15551, United Arab Emirates
[g] Department of Nanotechnology, Faculty of New Sciences and Technologies, Semnan University, Semnan, Iran

ARTICLE INFO

Handling editor. L Murr

Keywords:
AA2024 alloys
Accumulative roll bonding
Friction stir welding
Microstructure
Crystallographic texture
Hardness

ABSTRACT

The current research provides an insight into the correlation between the crystallographic textures, microstructure, and hardness of friction stir welded joints in nanostructured AA2024 alloys processed through accumulative roll bonding (ARB). Utilizing varying rotational speeds (250, 500, 750, and 1000 rpm) at a constant traverse tool (150 mm/min) during friction stir welding (FSW), microstructural analyses reveal distinct grain structures and texture components in the nugget zone. The fully recrystallized Cube {001}⟨100⟩ texture-oriented grains appear at the rotational speed of 750 rpm. The hardness profiles of ARB-processed strips after FSW at different rotational speeds show local softening in the nugget zones. There might be a hypothesis concerning the dissolution of stable and metastable precipitates based on generated heat input, providing insights into the mechanisms influencing hardness variations. Notably, the examination of Cube {001}⟨100⟩ texture and its correlation with local softening adds a valuable dimension to the understanding of microstructural changes in FSW of nanostructured AA2024 alloys processed by accumulative roll bonding process.

1. Introduction

Weight reduction without compromising safety performance is a major challenge in the automotive industry for improving fuel efficiency and reducing pollution. Reports indicate that aluminum alloys with several distinct characteristics such as being environmentally friendly, good weldability, high strength, and corrosion resistance are potential prospects for replacing identical steel assemblies, and their use in the automobile industry has lately increased [1,2]. Hence, it is vital to investigate efficient joining methods for replacing steel with aluminum alloys in automotive structures. Friction stir welding (FSW) was invented in 1991 to be an attractive solid state welding technique for aluminum alloy joining [3].

Nowadays, the focus is on nanostructured aluminum alloys, as they've been found to have superior mechanical properties in terms of strength and ductility and superior resistance to wear and corrosion [4–10]. The application of severe plastic deformation (SPD) to metals provides the potential for achieving exceptional grain refinement in bulk metal solids. Accumulative roll bonding (ARB) is a major SPD process for manufacturing sheet nanostructured materials and has an advantage for mass production because it can be carried out easily using conventional rolling apparatus [11,12]. Therefore, the welding of ARB-processed aluminum alloy sheets to produce a larger size has become very important. Obviously, the nanostructured material cannot be welded by

* Corresponding author. South Ural State University, 76 Lenin Av., Chelyabinsk 454080, Russia.
** Corresponding author. Brunel University London, Uxbridge, UB8 3PH, UK.
*** Corresponding author. United Arab Emirates University, Al-Ain 15551, United Arab Emirates.
**** Corresponding author. Semnan University, Semnan, Iran.
E-mail addresses: majid_na3ri@yahoo.com, naserim@susu.ru (M. Naseri), seyedmehdi.hosseini@brunel.ac.uk (S. Hosseini), ahmourad@uaeu.ac.ae (A.-H.I. Mourad), e.borhani@semnan.ac.ir (E. Borhani).

https://doi.org/10.1016/j.jmrt.2023.12.239
Received 22 November 2023; Received in revised form 24 December 2023; Accepted 25 December 2023
Available online 26 December 2023

the commonly used fusion welding process, since the molten pool generated during the welding will inevitably destroy the structure. In the aforementioned field, understanding the material flow during different stages of FSW is crucial for achieving optimized welding parameters and obtaining highly efficient welds. Material flow during FSW of nanostructured materials has been reported in the literature. Sato et al. [13] reported a decrease in the hardness of the nugget zone of ARB-processed aluminum alloy sheets, attributing it to grain growth in this zone. Khorrami et al. [14,15] have investigated the severely plastic deformed aluminum sheets joined by FSW at different welding conditions, such as rotational and traverse speeds. In their research, a reduction in hardness was noticed in the nugget zone compared to that of base metal due to thermal instability resulting from high stored energy during constrained groove pressing (CGP). Moreover, the strength of specimens was reduced with an increase in rotational speed due to the grain growth phenomenon.

It is well recognized that further efforts are needed to enhance the understanding of FSW. The evolution of microstructure and texture, along with the distribution and density of precipitates in different regions of welding joints, significantly influence their mechanical properties [16–19]. Therefore, studying the detailed correlation of these features is essential. To the best of our knowledge, the present work is the first of its kind to focus on the effect of cube {001}⟨100⟩ texture on the local softening of friction stir-welded joints for AA2024 alloys deformed to a high strain by the accumulative roll bonding process.

2. Experimental procedures

Fully annealed sheets of AA2024 alloy with an average grain size about 25 μm and an equiaxed grain structure served as the base alloy in this study. Two sheets of 150^{L} mm × 50^{W} mm × 0.8^{T} mm were degreased with acetone and scratch brushed with a stainless steel wire brush. Then, the prepared surfaces of the sheets were aligned, placed on top of each other, and secured at both ends with copper wires. The roll bonding process was conducted without lubrication at room temperature, resulting in a thickness reduction of 50 %. Then, the roll bonded sheets were cut into two pieces. This procedure described was repeated up to eight cycles. To join the sheets, specimens processed through eight ARB cycles were butt-welded using an FSW machine. The FSW tool, constructed from hot work tool steel, comprises a shoulder approximately 20 mm in diameter and a cylindrical pin with dimensions of 6 mm in width and 0.6 mm in length. FSW was conducted at a traveling speed of 150 mm/min and various rotational speeds (250, 500, 750, and 1000 rpm) in the rolling direction (RD). The heat input during FSW was calculated using Eqs (1) and (2) [20,21]:

$$Heat\ input\ (J/mm) = \frac{Power}{Speed} = \eta\frac{\omega T}{\nu} \tag{1}$$

$$\omega = \frac{2\pi r}{60} \tag{2}$$

where T is the torque (N.m), ω is the rotational speed (rpm), ν=*150* is the linear speed (mm/min), and η is the efficiency of heat transfer, (η = 0.9). The pseudo heat index is represented by the ratio of the square of the rotational speed to travel speed (ω^2/ν).

Microstructure characterization was conducted by scanning transmission electron microscopy (STEM, JEOL JEM-2100F) and electron back scattered diffraction (EBSD) in a field emission scanning electron microscope (FESEM). In preparation for STEM characterization, a focus ion beam (FIB) Helios G4 Thermo Fisher Scientific apparatus was used. To reduce noise in the STEM images presented herein, inverse fast Fourier transforming (IFFT) was performed with Gatan Digital Micrograph™ software. The specimen morphology was determined by transmission Kikuchi diffraction (TKD) with 15 kV and 6.4 nA settings in the FIB system. The sheets' normal direction (ND) was used as the reference axis for all inverse pole figure (IPF) maps. The acquired EBSD data to investigate the grain morphology and crystallographic texture was analyzed by TSL OIM ™ (EDAX, USA) software, and all the misorientation angles (θ) of approximately 2° were removed. $2^\circ \le \theta < 15^\circ$ and $\theta \ge 15^\circ$ were determined as low angle grain boundary (LAGB) and high angle grain boundary (HAGB), respectively.

Vickers microhardness profiles were measured on the transverse cross-section of joints. The measurements were carried out on the middle thickness of joints with an interval of 1 mm under a load of 100 g for 10 s.

3. Results and discussion

In Fig. 1, the microstructure of the starting material after 8 cycles of the ARB reveals a combination of elongated pancake-shaped ultrafine-grain microstructure, mostly surrounded by high-angle boundaries (f_{HAGBs} = 67 %) and misorientation of 34.57°. The average thickness of grains parallel to the transverse direction (TD) is less than 200 nm, while the mean length of the grains in RD is about 1 μm. Furthermore, the second-phase S-type precipitates are predominantly dispersed along the grain boundaries. The representative selected area diffraction (SAD) pattern in the STEM image also confirms the existence of submicron microstructure in the micrograph.

Fig. 2 illustrates that the microstructure of the starting materials changes in the stir/nugget zone as the rotational speed of the FSW tool increases. This evolution has been depicted using the EBSD inverse pole figure (IPF) maps. In Fig. 2a, although the f_{HAGBs} (76 %) have increased after FSW with a rotational speed of 250 rpm, the overall microstructure and misorientation remain relatively unchanged compared to the initial state. This suggests that the heating input (127.5 J/mm) provided by 250 rpm is not sufficient to initiate recrystallization. A similar microstructure is observed when the rotational speed is enhanced to 500 rpm (Fig. 2b). However, the dominance of f_{HAGBs} decreases in the resultant microstructure, and the misorientation parameter drops to 23.57°, indicating that partial recrystallization of the elongated grains begins when the rotational speed is 500 rpm and the heat input is 255 J/mm. As shown in Fig. 2c, a higher rotational speed (750 rpm) results in an equiaxial grain structure due to the complete recrystallization process driven by a frictional heat input of 282.5 J/mm. The grains in the nugget zone still have a submicron size, while the f_{HAGBs} and misorientation reach the maximum values of 84 % and 35.62°, respectively. Increasing the rotational speed and resultant heat input to 1000 rpm and 510 J/mm, respectively, leads to the activation of the grain growth phenomenon after recrystallization of the elongated grains in Fig. 2d. The f_{HAGBs} (76 %) and misorientation (32.10°) values are similar to those of the specimen welded with a rotational speed of 250 rpm but lower than the corresponding features in the fully recrystallized nugget zone of the specimen with rotational speed of 750 rpm.

The dynamic recrystallization in the nugget region is primarily a result of two converging effects: the heat input produced by the stirring tool and the severe deformation caused by the stirring pin. The high strain rate due to the high rotational speed of the pin lowers the recrystallization temperature, thereby accelerating the growth of the grains [22,23]. In this study, the tool traverse speed was kept constant at 150 mm/min while the rotational speed was varied. Therefore, the welding time remains constant for all the specimens, while the strain rate and frictional heat input increase with enhancing the rotational speed. This is the reason why fully recrystallization and grain growth are observed in the welded specimens with a rotational speed of 750 and 1000 rpm, respectively. It is noteworthy to mention that the mean size of recrystallized grains (Fig. 2c) is much lower than that reported in the literature for non-hardenable Al alloys after FSW [17,22]. The reason can be attributed to the contributing of the fine second-phase particles attached to grain boundaries, which are effective in prohibiting grain growth. Another reason is most likely ascribed to a sort of secondary severe plastic deformation taking place at a rotational speed of 750 rpm, leading to an appropriate material flow in the nugget zone, as the

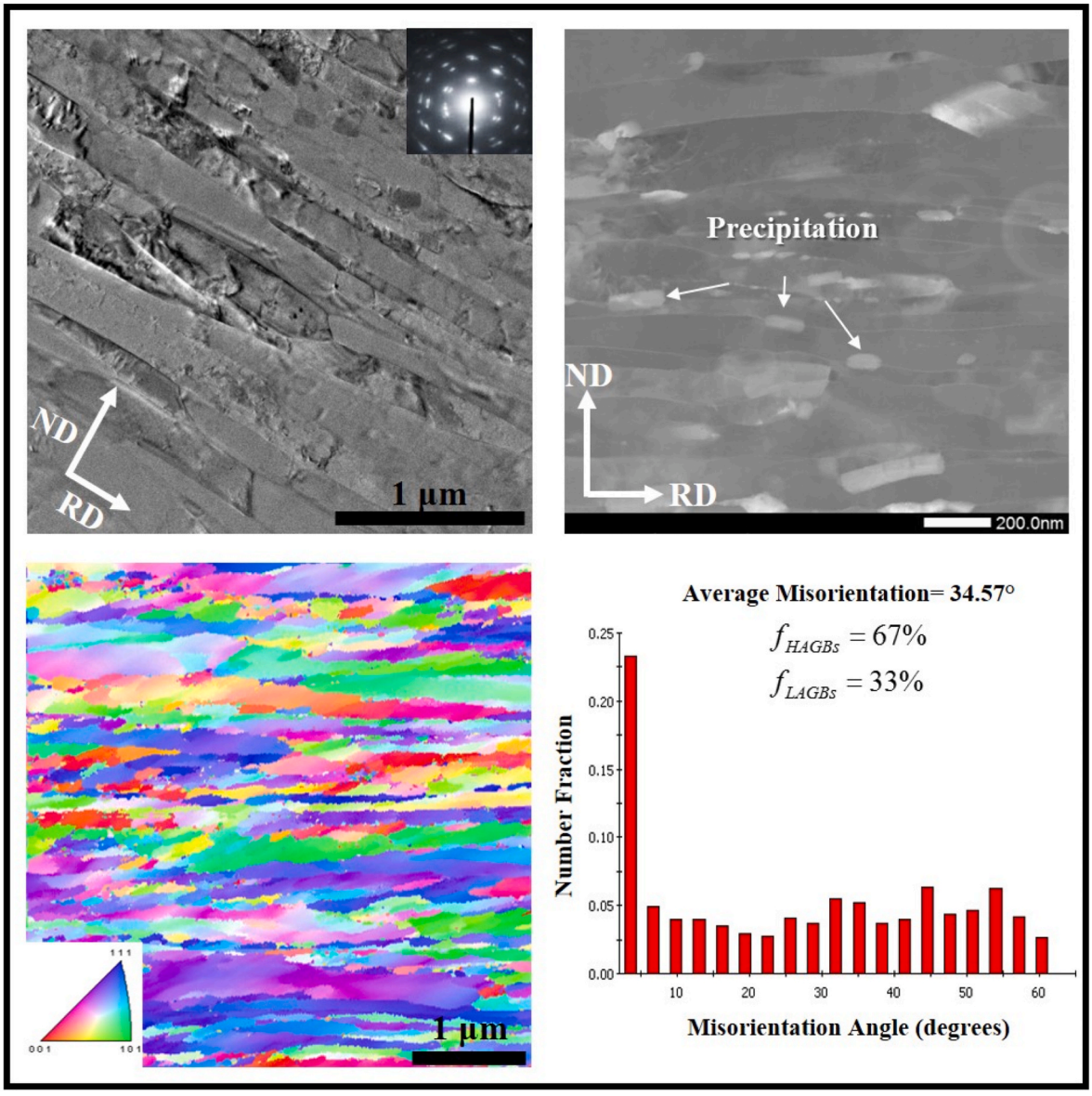

Fig. 1. STEM micrographs and the matching SAD pattern, EBSD inverse pole figure (IPF) map and misorientation angle distribution from the RD–ND plane of AA2024 alloy after eight ARB cycles.

maximum f_{HAGBs} and misorientation values were achieved under this condition.

Fig. 3 illustrates the orientation distribution functions (ODFs) at constant angles (φ2) of 0°, 45°, and 65° for the stir zone at different welding conditions. As shown in Fig. 3a, the initial texture of the strips after ARB is Copper {112}⟨111⟩, P {110}⟨221⟩, and S {123}⟨634⟩ with the maximum intensities of 15.4 × R, 12.3 × R, and 10.6 × R, respectively. Notably, the intensities and/or texture components of the nugget zone alter with various tool speeds. In Fig. 3b, corresponding to a rotational speed of 250 rpm, lower intensities of texture components described for the ARBed specimens are observed. With the increase in heat input due to the rotational speed rising to 500 rpm (Fig. 3c), Cube-oriented grains might develop through the rotation of Copper-oriented grains towards the fiber or from the S-component with a preferred growth relationship 38° around <111>. The corresponding microstructure (Fig. 2c) shows Cube-oriented grains between the elongated grains characterized by the S-component. The maximum intensity of both Cube {001}⟨100⟩ and S {123}⟨634⟩ components is measured 2.5 × R, indicating the disappearance of Copper {112}⟨111⟩ and P {110}⟨221⟩ components and a dramatic intensity reduction of the S {123}⟨634⟩ component. In Fig. 3d, Cube {001}⟨100⟩ and Rt Cube {001}⟨110⟩ components with maximum intensities of 3.1 × R and 2.4 × R are dominant in the nugget zone. In fact, these texture components accelerate the formation of equiaxed and fine grains in the nugget zone by dynamic recrystallization (DRX) [24–27], which is in good agreement with microstructural observations in Fig. 2c. At a rotation speed of 1000 rpm (Fig. 3e), P {011}⟨221⟩ component with a maximum intensity of 6.6 × R is identified as the texture of the nugget zone. It has been reported that Cube {001}⟨100⟩ and Rt Cube {001}⟨110⟩ components can be transformed into orientations on α-fiber around the stable Brass {011}⟨211⟩, including G/B {110}⟨115⟩, G/B_T {110}⟨111⟩, and P {011}⟨221⟩ in aluminum alloys where heat input is more than the values required for the establishing the components attributed to the fully recrystallized microstructure [26,28,29].

In the FSW of materials, the critical issue is the sheet positioning concerning the tool rotation direction, which can provide superior tensile properties and a defect-free welded joint. The similar direction of the tangential component of the rotating tool and the tool traverse direction on the advancing side (AS) produces additional frictional heat compared to the retreating side (RS), where the tool rotation direction is opposite

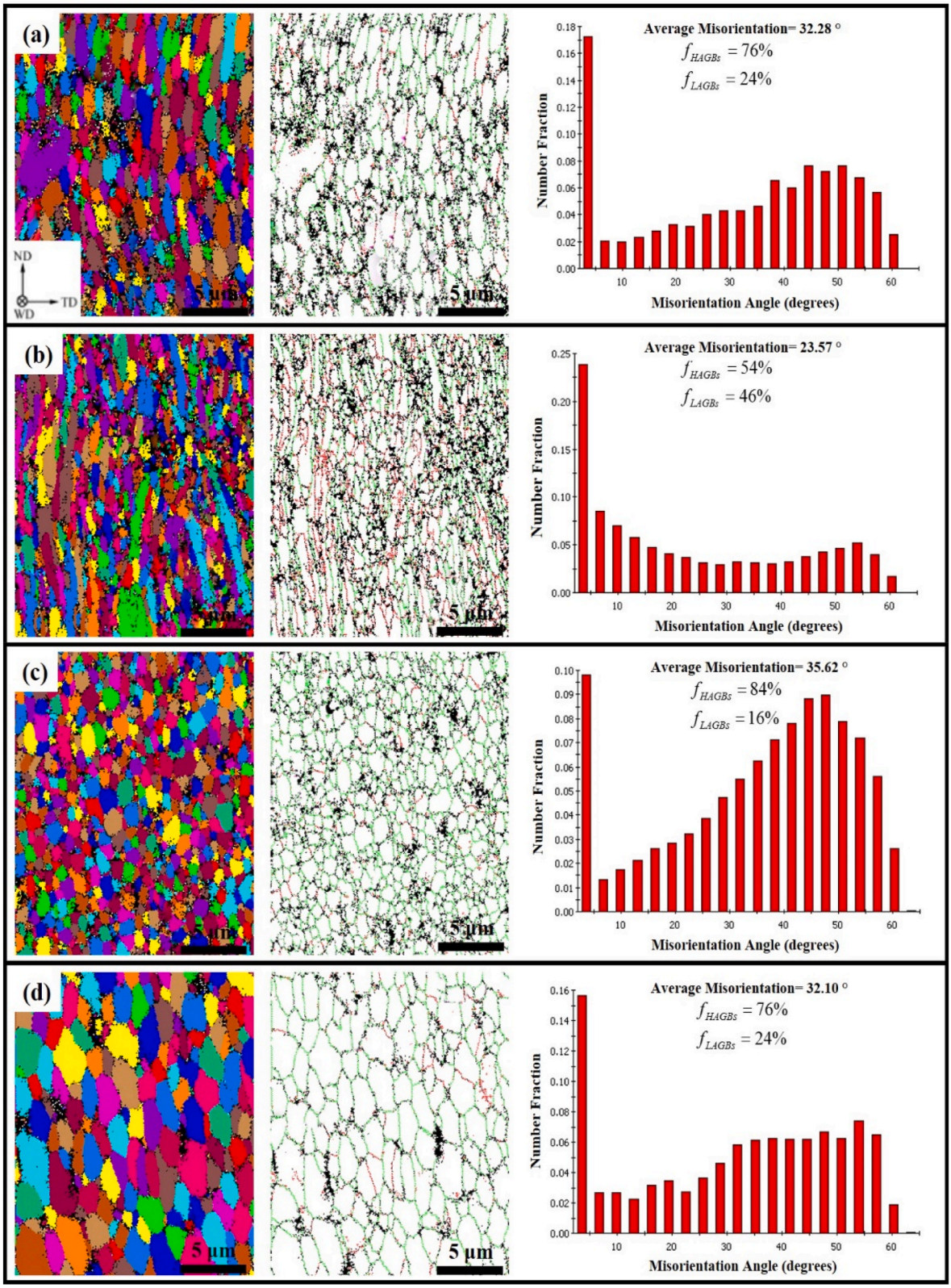

Fig. 2. EBSD inverse pole figure (IPF) maps and misorientation angle distribution of the stir zone in the friction stir welding of the ARB-processed AA2024 alloy joint obtained by different welding conditions, (a) 250 rpm/150 mm/min, (b) 500 rpm/150 mm/min, (c) 750 rpm/150 mm/min, and (d) 1000 rpm/150 mm/min.

that of the tool traverse direction. The hardness profile of the annealed and ARB-processed strips before and after FSW at different rotational tool speeds, from the base material to nugget zone, is depicted in Fig. 4. Local softening of the hardness profiles in the nugget zones is evident, regardless of whether the grain size increases or decreases due to FSW, as discussed for Fig. 2c and d. However, specimens manufactured with a 1000 rpm rotational speed showed the highest degree of softening, while the fully recrystallized nugget zone with a dominant Cube {001}⟨100⟩

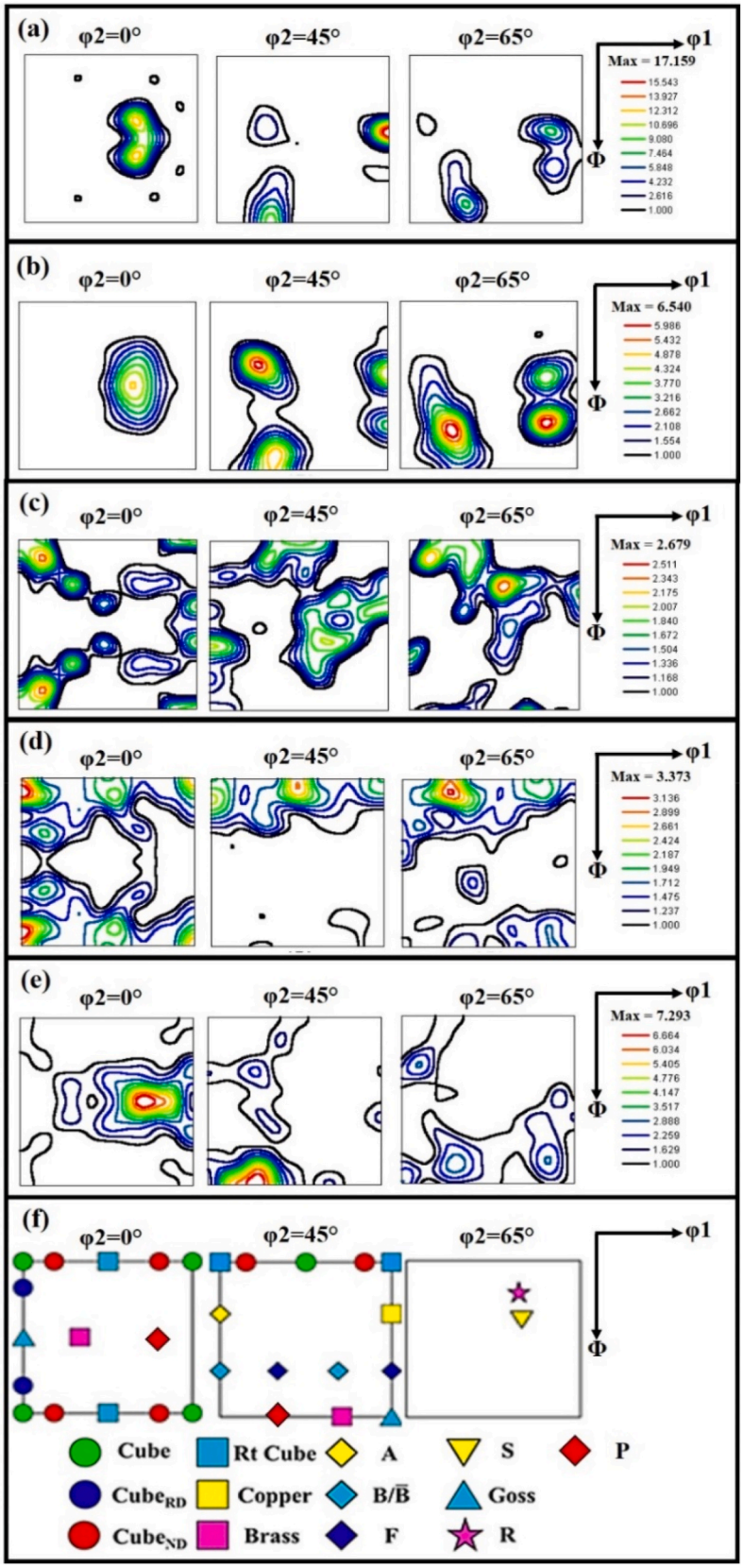

Fig. 3. ODFs at constant angles (0°, 45°, and 65°) of the stir zone in the friction stir welding of the ARB-processed AA2024 alloy joint obtained by different welding conditions: (a) ARB-processed AA2024 (base material), (b) 250 rpm/150 mm/min, (c) 500 rpm/150 mm/min, (d) 750 rpm/150 mm/min, and (e) 1000 rpm/150 mm/min, and (f) main ideal positions of texture components of FCC materials.

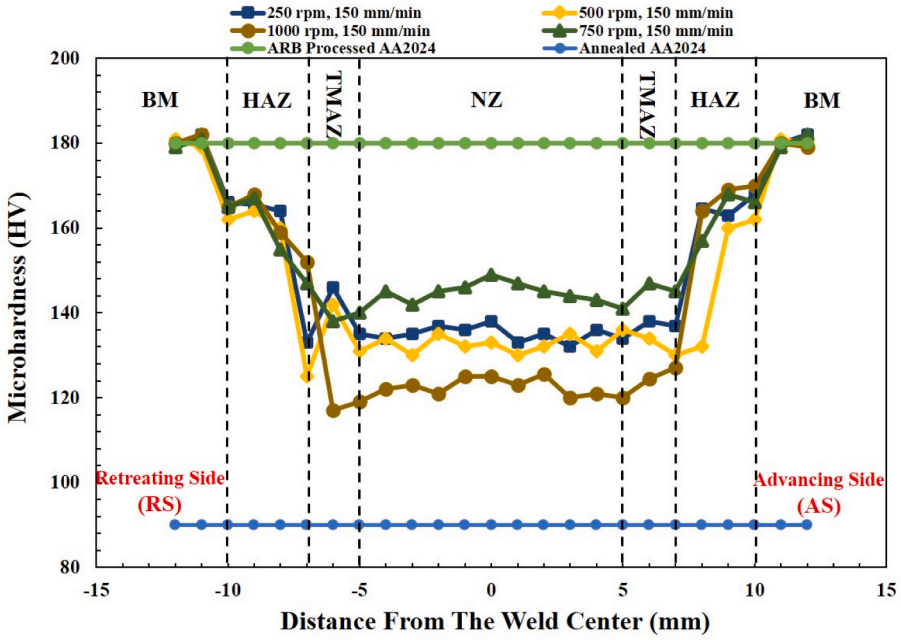

Fig. 4. Microhardness distribution across the stir zone of the four joints, base material and starting material for FSW specimens.

texture, produced by 750 rpm rotational speed, experienced the lowest local softening. The two other conditions revealed relatively similar hardness profiles, falling between the lowest and highest hardness profiles, although the average hardness value of the specimen in nugget zone with a 250 rpm rotational speed was slightly higher.

The local softening of the nugget zone can be attributed to the partial or fully recrystallized microstructure in the nugget and complex variations in the number density, morphology and distribution of the S-type precipitates [13,30,31]. Two hypotheses are proposed to analyze this occurrence. The first posits that the complete dissolution of precipitates and re-precipitation within the nugget lead to slightly higher hardness in the nugget than in the thermo-mechanically affected zone (TMAZ) [22,23]. This theory aligns with specimens with higher heat input in FSW strips done at 750 rpm (282.5 J/mm) and 1000 rpm (510 J/mm) rotational speeds. In other words, the second argument suggests that the heat input in the nugget is not adequately high to dissolve the stable precipitates and might only be enough to dissolve the metastable ones, as seen in FSW specimens produced at 250 rpm (127.5 J/mm) and 500 rpm (255 J/mm) rotational speeds. It can be stated that the heat provided by the 750 rpm rotational speed results in a fully recrystallized grain with the Cube {001}⟨100⟩ texture and most likely manipulated precipitates, representing the lowest loss of hardness of the nugget zone in ARB-processed FSW specimens.

4. Conclusions

The study investigated the microstructural changes in the nugget zone of the nanostructured AA2024 alloys processed through accumulative roll bonding (ARB) and subsequent friction stir welding (FSW). Analyses revealed a distinct starting material microstructure characterized by ultrafine grains, high-angle boundaries, and S-type precipitates. FSW at varied rotational speeds induced microstructural evolution in the stir/nugget zone, impacting grain structures and orientations. The dynamic recrystallization in the nugget region, driven by appropriate heat input and severe deformation, exhibited crystallographic texture of Cube-type {001}⟨100⟩ component at rotational speed of 750 rpm. The hardness profiles displayed local softening in nugget zones, with the highest softening in 1000 rpm specimens and the least in fully recrystallized nugget zones at 750 rpm. It was concluded that the complex variations in S-type precipitates can influence the nugget zone's hardness. Overall, the findings contribute to understanding the delicate interactions of crystallographic texture, microstructure, and hardness profile in ARB-processed FSW of nanostructured AA2024 alloys.

CRediT authorship contribution statement

Majid Naseri: Conceptualization, Investigation, Validation, Writing - original draft, Writing - review & editing, Project administration. **Mohammad Alvand:** Investigation, Validation. **Ehsan Ahmadi:** Investigation, Validation, Writing - original draft. **Seyedmehdi Hosseini:** Conceptualization, Validation, Writing - original draft, Writing - review & editing. **Davood Gholami:** Investigation, Validation, Writing - review & editing. **Abdel-Hamid I. Mourad:** Validation, Writing - original draft, Writing - review & editing. **Ehsan Borhani:** Conceptualization, Validation.

Declaration of competing interest

The authors declare that they have no known competing financial interests or personal relationships that could have appeared to influence the work reported in this paper.

Acknowledgment

M. Naseri is grateful to Seoul National University, Seoul, South Korea, for the use of facilities in the Department of Materials Science and Engineering under the Brain Korea 21 (BK21) Postdoctoral Fellowship. He is also most appreciative of Prof. H.W. Jang and Prof. M.R. Shokouhimehr for informative discussion and technical assistance in FIB-TEM and EBSD experiments.

References

[1] Li SS, Yue X, Li QY, Peng HL, Dong BX, Liu TS, Yang HY, Fan J, Shu SL, Qiu F, Jiang QC. Development and applications of aluminum alloys for aerospace industry. J Mater Res Technol 2023;27:944–83.
[2] Cann JL, De Luca A, Dunand DC, Dye D, Miracle DB, Oh HS, Olivetti EA, Pollock TM, Poole WJ, Yang R, Tasan CC. Sustainability through alloy design: Challenges and opportunities. Prog Mater Sci 2021;117:100722.

[3] Dawes CJ, Thomas WM. Friction stir joining of aluminum alloys. TWI Bulletin, The Welding Institute; 1995. p. 124–7.
[4] Naseri M, Hassani A, Tajally M. An alternative method for manufacturing Al/B_4C/SiC hybrid composite strips by cross accumulative roll bonding (CARB) process. Ceram Int 2015;41(10, Part A):13461–9.
[5] Naseri M, Reihanian M, Borhani E. Effect of strain path on microstructure, deformation texture and mechanical properties of nano/ultrafine grained AA1050 processed by accumulative roll bonding (ARB). Mater Sci Eng 2016;673:288–98.
[6] Naseri M, Reihanian M, Moghaddam AO, Gholami D, Hosseini S, Alvand M, Borhani E, Trofimov E. Improving strength-ductility synergy of nano/ultrafine-structured Al/Brass composite by cross accumulative roll bonding process. J Mater Res Technol 2023;26:6794–806.
[7] Alvand M, Naseri M, Borhani E, Abdollah-Pour H. Nano/ultrafine grained AA2024 alloy processed by accumulative roll bonding: a study of microstructure, deformation texture and mechanical properties. J Alloys Compd 2017;712 (Supplement C):517–25.
[8] Naseri M, Reihanian M, Borhani E. A new strategy to simultaneous increase in the strength and ductility of AA2024 alloy via accumulative roll bonding (ARB). Mater Sci Eng 2016;656:12–20.
[9] Jamaati R, Naseri M, Toroghinejad MR. Wear behavior of nanostructured Al/Al_2O_3 composite fabricated via accumulative roll bonding (ARB) process. Mater Des 2014;59:540–9.
[10] Fattah-alhosseini A, Naseri M, Alemi MH. Corrosion behavior assessment of finely dispersed and highly uniform Al/B_4C/SiC hybrid composite fabricated via accumulative roll bonding process. J Manuf Process 2016;22:120–6.
[11] Saito Y, Tsuji N, Utsunomiya H, Sakai T, Hong RG. Ultra-fine grained bulk aluminum produced by accumulative roll-bonding (ARB) process. Scripta Mater 1998;39(9):1221–7.
[12] Tsuji N, Saito Y, Utsunomiya H, Tanigawa S. Ultra-fine grained bulk steel produced by accumulative roll-bonding (ARB) process. Scripta Mater 1999;40(7):795–800.
[13] Sato YS, Kurihara Y, Park SHC, Kokawa H, Tsuji N. Friction stir welding of ultrafine grained Al alloy 1100 produced by accumulative roll-bonding. Scripta Mater 2004; 50(1):57–60.
[14] Sarkari Khorrami M, Kazeminezhad M, Kokabi AH. Thermal stability during annealing of friction stir welded aluminum sheet produced by constrained groove pressing. Mater Des 2013;45:222–7.
[15] Sarkari Khorrami M, Kazeminezhad M, Kokabi AH. Microstructure evolutions after friction stir welding of severely deformed aluminum sheets. Mater Des 2012;40: 364–72.
[16] Verma J, Padap AK. Evolution of microstructure and mechanical characteristics of friction stir welded ultrafine-grained aluminum alloy 6082. Mater Werkst 2023;54 (8):1003–13.
[17] Roy S, D SS, Suwas S, Kumar S, Chattopadhyay K. Microstructure and texture evolution during accumulative roll bonding of aluminium alloy AA5086. Mater Sci Eng 2011;528(29):8469–78.
[18] Topic I, Höppel HW, Göken M. Friction stir welding of accumulative roll-bonded commercial-purity aluminium AA1050 and aluminium alloy AA6016. Mater Sci Eng 2009;503(1):163–6.
[19] Chen Y, Xiong C, Liu W, Pan S, Song Y, Liu Y, Zhu B. Texture evolution and Control of 2524 aluminum alloy and its effect on fatigue crack propagation behavior. Appl Sci 2021;11(12):5550.
[20] Kumar R, Singh K, Pandey S. Process forces and heat input as function of process parameters in AA5083 friction stir welds. Trans Nonferrous Metals Soc China 2012; 22(2):288–98.
[21] Ahmed M, Wynne B, Rainforth W, Addison A, Martin J, Threadgill P. Effect of tool geometry and heat input on the hardness, grain structure, and crystallographic texture of thick-section friction stir-welded aluminium. Metall Mater Trans 2019; 50:271–84.
[22] Lipińska M, Olejnik L, Pietras A, Rosochowski A, Bazarnik P, Goliński J, Brynk T, Lewandowska M. Microstructure and mechanical properties of friction stir welded joints made from ultrafine grained aluminium 1050. Mater Des 2015;88:22–31.
[23] Zhou Y, Xiong H, Zhang Y, Kong C, Yu H. Microstructure and mechanical properties of ultrafine-grained AA2024 sheets joined by underwater friction stir welding. Mater Char 2023;198:112749.
[24] Weimin M. Recrystallization and grain growth, encyclopedia of aluminum and its alloys. CRC Press; 2018.
[25] Tolouei E, Toroghinejad MR, Asgari H, Monajati Zadeh H, Ashrafizadeh F, Szpunar JA, Bocher P. Microstructure and texture development in Al–3% Brass composite produced through ARB. Adv Eng Mater 2018;20(4):1700463.
[26] Naseri M, Borhani E, Imantalab O, Jang HW, Shokouhimehr M, Fattah-alhosseini A. Correlation between crystallographic texture and electrochemical behavior of nano/ultrafine-grained AA2024 alloy processed by accumulative roll bonding process. J Mater Res Technol 2022;18:4256–66.
[27] Chen YQ, Xu JB, Pan SP, Lu DD, Song YF, Liu Y, Zhi Q, Liu HQ. Effects of initial orientation on microstructure evolution of aluminum single crystals during hot deformation. Mater Sci Eng 2023;883:145502.
[28] Harati F, Shamanian M, Atapour M, Hasani S, Szpunar J. The effect of microstructure and texture evolution on the hardness properties of the cold rolled AA7075-T6 aluminum alloy during the friction stir processing. Mater Res Express 2019;6(4):046559.
[29] Shen F, Zhou Z, Li W, Sun Z, Tian J, Xie C, Guo J, Liao Z, Yi D, Zhang J. Micro-mechanism of texture evolution during isochronal annealing of as-annealed hot rolled Al-Cu-Mg sheet. Mater Des 2019;165:107575.
[30] Morita T, Yamanaka M. Microstructural evolution and mechanical properties of friction-stir-welded Al–Mg–Si joint. Mater Sci Eng 2014;595:196–204.
[31] Cerri E, Leo P, Wang X, Embury JD. Mechanical properties and microstructural evolution of friction-stir-welded thin sheet aluminum alloys. Metall Mater Trans 2011;42(5):1283–95.